Key Note Talk: The 3rd International Symposium on Ubiquitous Knowledge Network Environment, Sapporo, Japan, February 2006

Microstructured Optical Fibers: Overview of Novel Materials and Geometries for Applications Beyond Telecom

Prof. Maksim Skorobogatiy
Canada Research Chair in
Photonic Crystals

www.photonics.phys.polymtl.ca

École Polytechnique de Montréal, Quebéc
CANADA

Microstructured Fiber Sensors

(by far not a complete overview)

- Absorption and Phase Change Based Sensors for Chemical Detection
- Temperature and Stress Change Sensors
- Resonant Sensors, Plasmonic Resonance Sensors

Absorption and Phase Change Based Sensors for Chemical Detection

Absorption and Phase Change Based Sensors

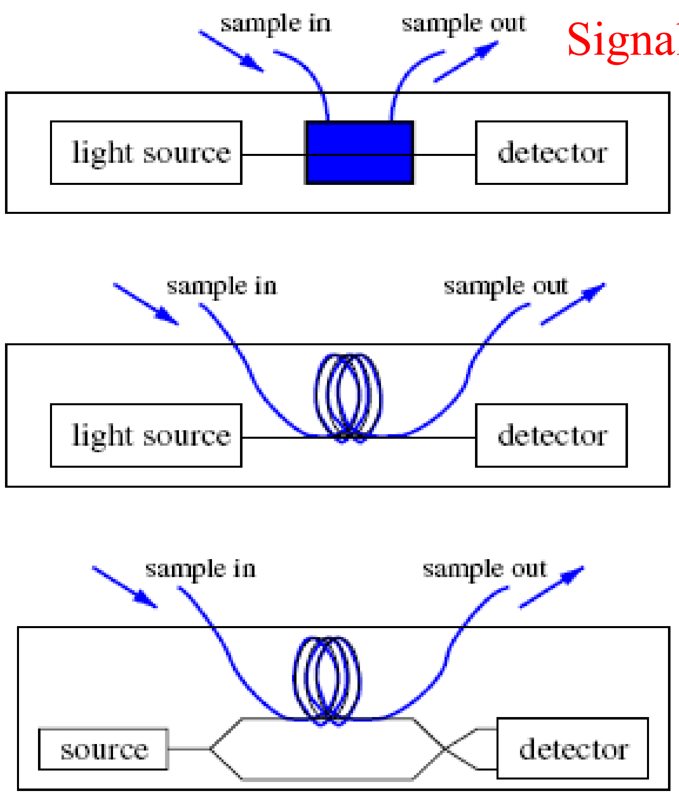

Figure 1. Optical fibre can dramatically improve the sensitivity of a sensor by increasing the interaction length between light and the sample. In a typical bulk configuration (top), light interaction with the sample may be limited to lengths of a few centimetres. We present specialty fibre designs that will allow interaction of guided light with a sample over a metre length and greater distances (middle). Interferometric detection of light (bottom) can also be used if mode-coupling in the waveguide can be controlled.

Signal ∝ (Interaction length) × (Overlap) × exp(− Loss×Length)

Overlap

$$\delta n_{\mathrm{eff}} \approx \frac{\int \mathrm{d}A\, \Delta\epsilon |\boldsymbol{E}|^2}{2\sqrt{\epsilon_0 \mu_0} \int \mathrm{d}A\, \mathcal{R}\{\boldsymbol{E}^* \times \boldsymbol{H}\} \cdot \hat{\boldsymbol{z}}},$$

$$\delta n_{\mathrm{eff}} \approx \delta n_{\mathrm{sample}} \frac{[\text{Power in analyte}]}{[\text{Total power}]}$$

Amplitude change ~ (Interaction length) ×Imag(δneff)

Phase change ~ (Interaction length) ×Real(δneff)

J.M. Fini, "Microstructure fibres for optical sensing in gases and liquids," Meas. Sci. Technol. **15**, 1120 (2004)

Group PolyPhotonique

Holey Fiber (HF) Absorption Based Sensors

Main idea – put analyte where the light is

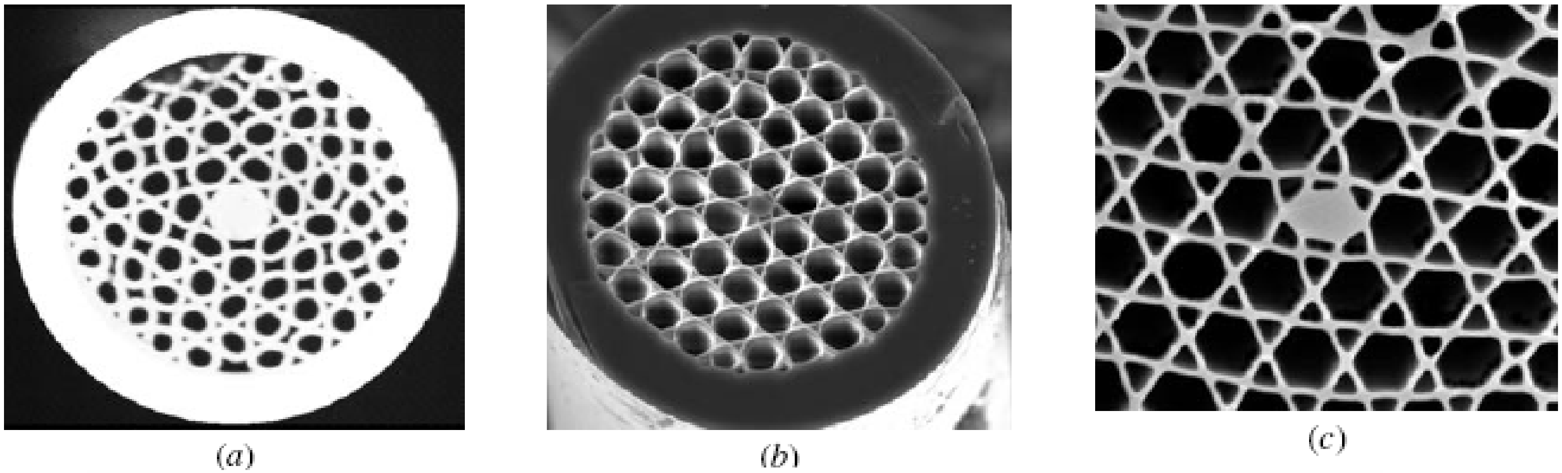

Figure 1. Three large air-filled holey optical fibres: (*a*) a large core HF (core diameter 45 μm), (*b*) a holey fibre with a 5 μm core and (*c*) a small core holey fibre with a 1.5 μm core.

The holes in the cladding of a HF open up new opportunities for exploiting the interaction of light with gases and liquids via evanescent coupling effects

T. Monro et al., "Sensing with microstructured optical Fibres," Meas. Sci. Technol. **12**, 854 (2001)

Holey Fiber (HF) Absorption Based Sensors

- The concentration of pollutants in a gas could be determined by measuring the absorption that occurs as light propagates through the gas
- Fiber based sensors can exhibit extremely long interaction lengths, while designed in a compact fashion (10s of meters) which is impossible to achieve in bulk samples.
- Tiny gas volumes are needed for measurement (nanoliters)
- Infinitely single mode HFs allow reliable sensing at widely different wavelengths
- In order for HFs to be superior to other evanescent field sensors, a significant fraction of the modal field must be located within the holes (>20%)
- Fiber propagation loss should be small to allow long sensors (fraction of a dB per meter)
- Gas filling time of HFs can be large due to very small holes

Group PolyPhotonique

Modal Absorption Loss in Gas Filled HFs

The evanescent field in the air holes is absorbed by the gas species, and the gas concentration can be obtained from the intensity attenuation through the Beer–Lambert law:

$$I(\lambda) = I_0(\lambda)\exp[-r\alpha_m(\lambda)lC].$$

I and *Io* are the output light intensities with and without the presence of gas being detected, αm is the bulk absorption coefficient of a gas being measured, *l* is the length of the HF sensor, *C* is the gas concentration and *r* is a relative sensitivity coefficient defined as:

$$r = (n_r/n_e)f,$$

where nr is the index of the gas ~ 1, ne is the effective index of the guided mode, and *f* is the fraction of the total power located in the holes. Power Fraction (PF) *f* can be calculated by integrating the optical power inside the air holes and dividing it by the total power carried by that mode

$$f = \int_{\text{holes}} (E_x H_y - E_y H_x)\mathrm{d}x\mathrm{d}y \Big/ \int_{\text{total}} (E_x H_y - E_y H_x)\mathrm{d}x\mathrm{d}y,$$

Y.L. Hoo et al., "Design and modeling of a photonic crystal fiber gas sensor," Appl. Opt. **42**, 3509 (2003)

Group PolyPhotonique

Improving HFs Detection Sensitivity

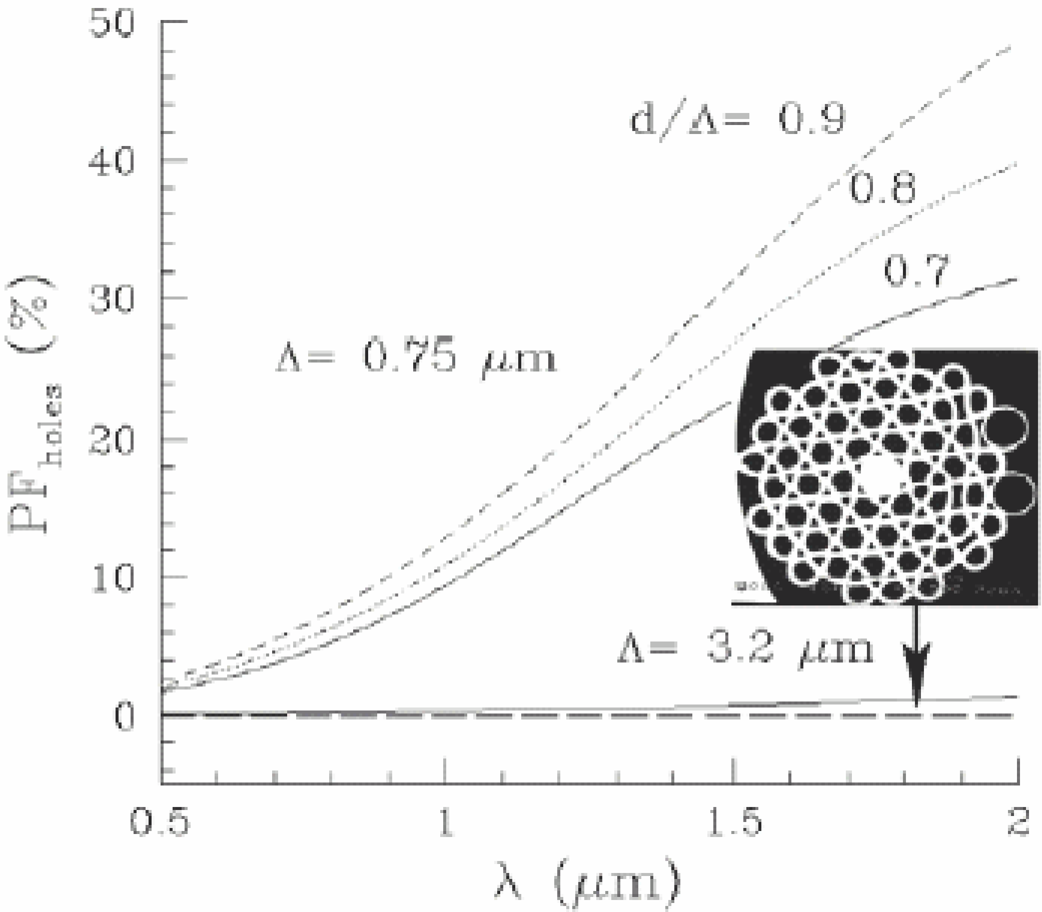

Figure 2. The fraction of the modal power located in the holes for a range of fibres. The inset shows a HF with a pitch of 3.2 μm.

Thinner Veins

Longer Wavelengths

T. Monro et al., "Sensing with microstructured optical Fibres," Meas. Sci. Technol. **12**, 854 (2001)

Group PolyPhotonique

ÉCOLE POLYTECHNIQUE MONTRÉAL

Core Design to Increase Sensitivity

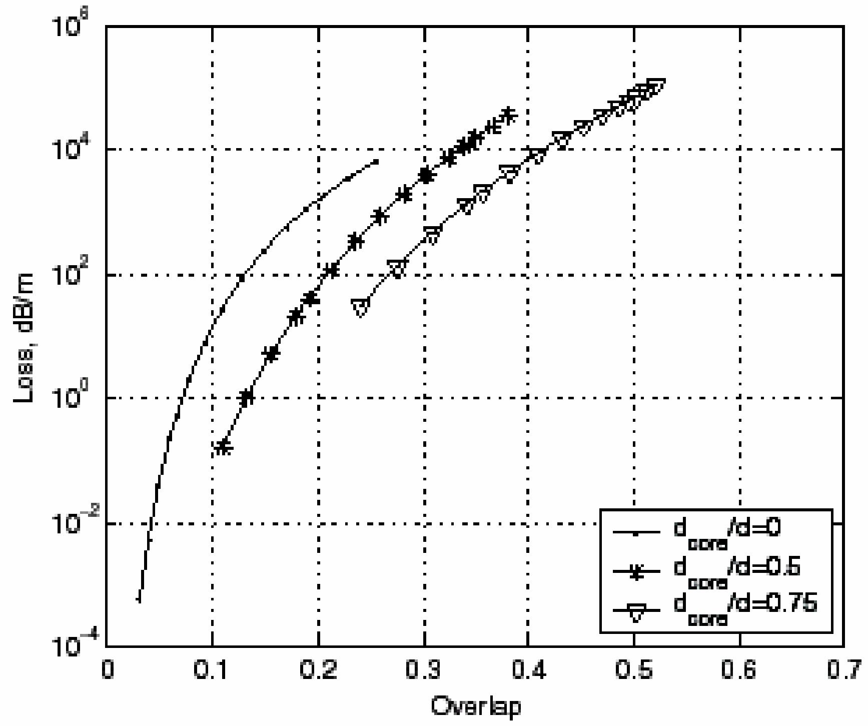

Figure 7. Modified evanescent-field fibre overlap plotted versus loss.

Air hole of diameter d

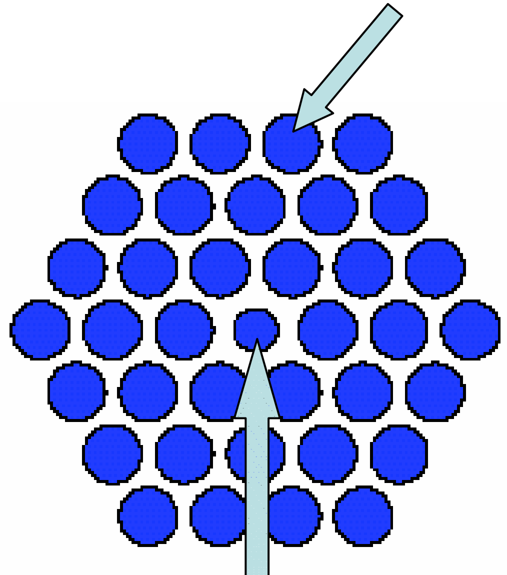

Figure 5. Modified evanescent-field geometry.

Air hole of diameter dcore<d in the core pushes the core mode into the porous cladding

J.M. Fini, “Microstructure fibres for optical sensing in gases and liquids,” Meas. Sci. Technol. **15**, 1120 (2004)

K. Saitoh, M. Koshiba, et al. Endlessly single-mode holey fibers: the influence of core design,’’ Opt. Express **13**, 10833 (2005)

Group PolyPhotonique

Sensor Response Time

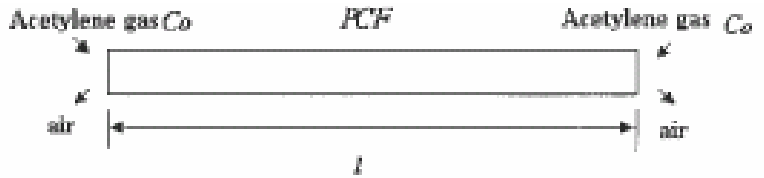

Fig. 5. Gas diffusion into the holes of the PCF of length l.

$$C(x,t) = C_0\left(1 - (4/\pi)\sum_{j=1,3,5}^{\infty}(1/j) \times \{\sin(j\pi x/l)\exp[-(j\pi/l)^2 Dt]\}\right),$$

One concern in using HFs as evanescent field sensors may be the limited response time due to the long time required for a gas to diffuse into the holes.

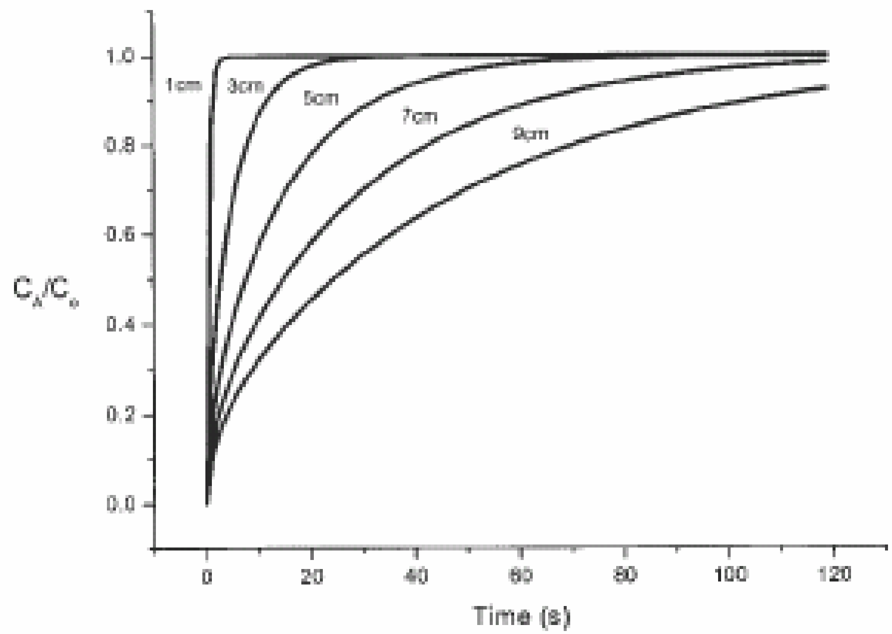

Fig. 6. Normalized average concentration inside the hole's column against the time for a range of fiber lengths l. Diffusion is assumed to be from both ends and with the wall effect considered.

When l is 1 m the time for C_2H_2 gas to reach 90% *Co* is 200 min. Pressure differencing of the fiber ends to decrease response time is hindered by very small hole sizes.

Y.L. Hoo et al., "Design and modeling of a photonic crystal fiber gas sensor," Appl. Opt. **42**, 3509 (2003)

Sensor Power Budget and Sensitivity

$$P_s - \alpha_f L - r\alpha_m C_{\max} L \geq P_D$$

αm=0.012 dB/m is the absorption coefficient of acetylene gas at 1.5315 μm

αf=0.1dB/m is the loss of the HF

r=13.7% is the relative sensitivity of a particular HF

P_s=5μW(7 dBm) is a typical input power

P_D=10nW(-50 dBm) is a detection threshhold

C_{max}=5% is maximum gas concentration – Sensor Range

The maximum sensor length is **L**= 4.87 m. This is equivalent to an open-path gas cell with an equivalent length of 4.87*13.72% =0.668 m

Sensor sensitivity for **L**= 4.87m of HF is ~ 6 parts per million

Y.L. Hoo et al., "Design and modeling of a photonic crystal fiber gas sensor," Appl. Opt. **42**, 3509 (2003)

Sensing Using Gas Filled Hollow Core Photonic Band Gap Fibers

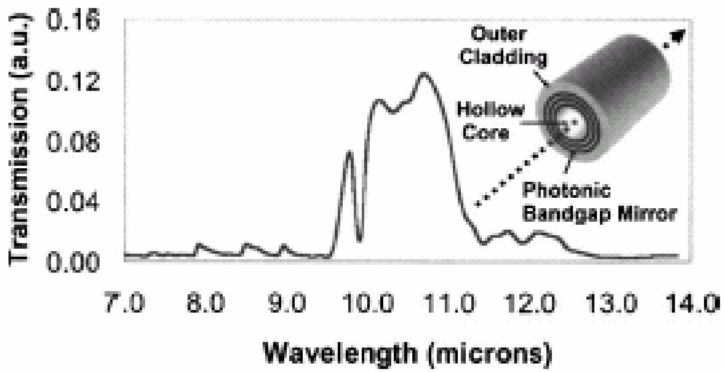

FIG. 1. FTIR transmission spectrum and schematics of the OmniGuide

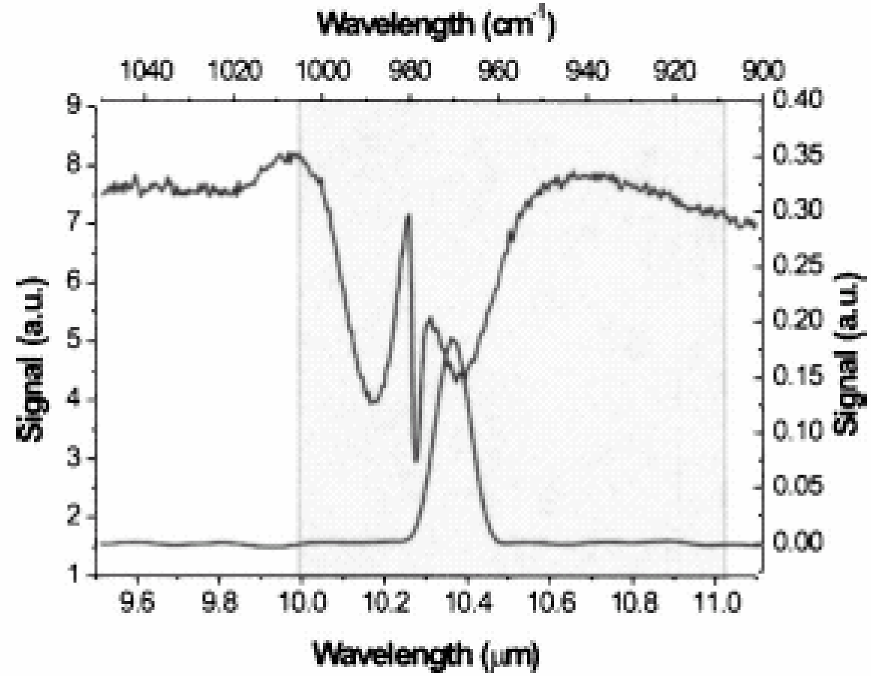

FIG. 2. 10.3 μm InGaAs/InAlAs/InP DFB-QCL emission spectrum (bottom), ethyl chloride absorption spectrum (top), and photonic band gap of the 10.6 μm OmniGuide Fiber (gray area). The spectrum of ethyl chloride was

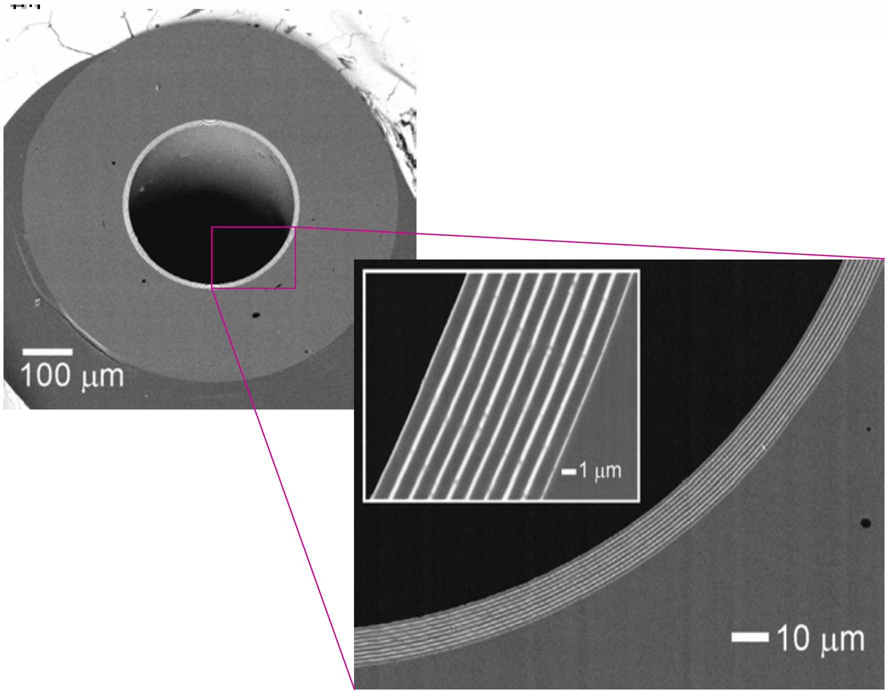

f=99 % of the guided mode field energy can propagate in the air regions of the gas filled fiber

Sensor sensitivity for **L**= 0.07m of HF is ~ 0.04 parts per million (compare wit 6 ppm of a HF)

C. Charlton et al., "Midinfrared sensors meet nanotechnology: Trace gas sensing with quantum cascade lasers inside photonic band-gap hollow waveguides," Appl. Phys. Lett. 86, 194102 (2005)

Gas Sensing Experimental Setup

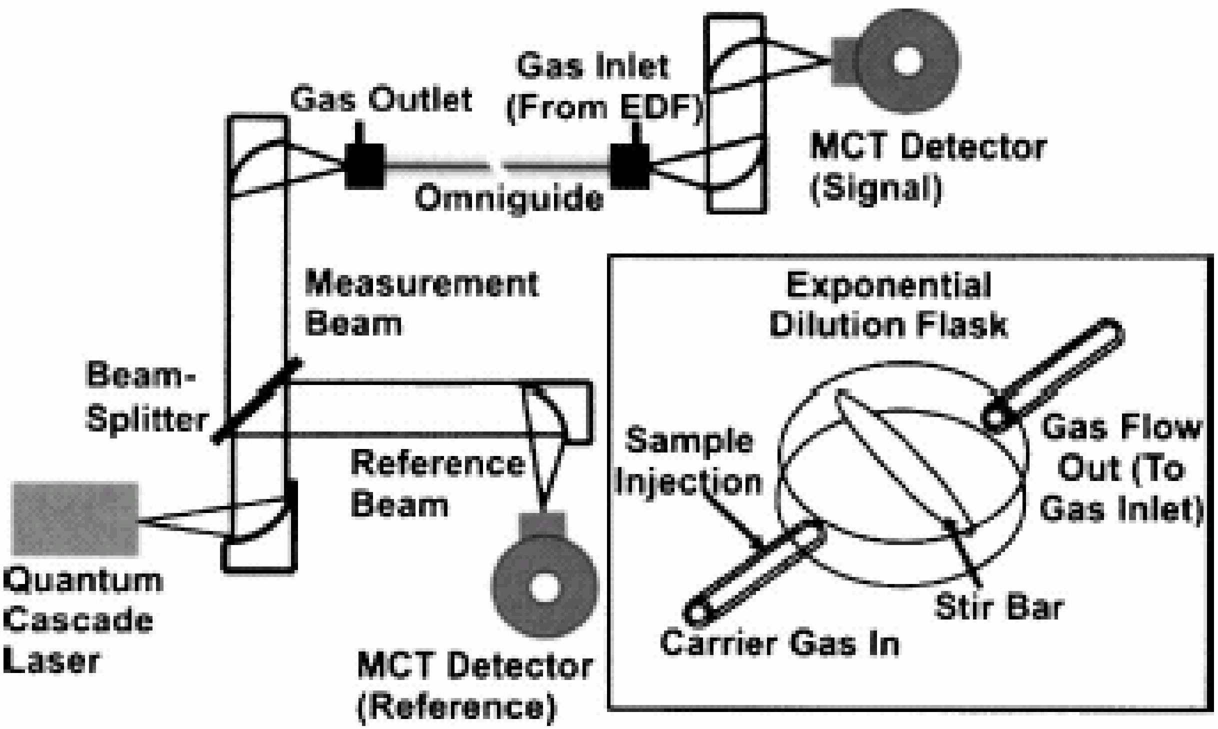

FIG. 3. Experimental setup with the laser radiation emitted from the QCL focused into an OmniGuide Fiber via custom made gas cells enabling simultaneous coupling of radiation and insertion of gaseous samples from the exponential dilution flask into the hollow waveguide; signals of the reference and the measurement channel are detected by MCT detectors (liquid-N_2 cooled) after focusing of the radiation with off-axis parabolic mirrors.

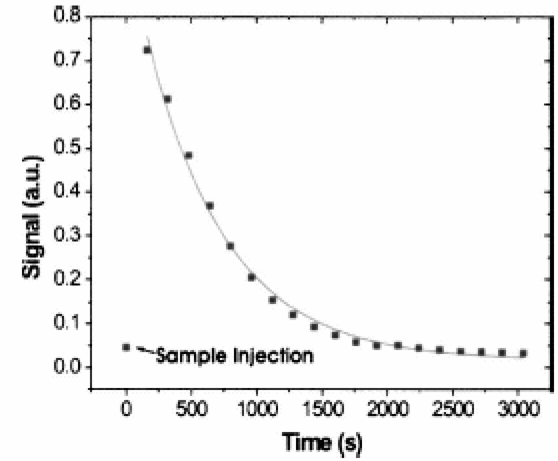

FIG. 4. Typical sensor response curve resulting from the interaction of the exponentially diluted ethyl chloride gas sample continuously flowing at 39 mL/min through the photonic band-gap gas cell with radiation emitted from the QCL light source.

Sensor calibration using Exponential Dilution Flask

C. Charlton et al., "Midinfrared sensors meet nanotechnology: Trace gas sensing with quantum cascade lasers inside photonic band-gap hollow waveguides," Appl. Phys. Lett. 86, 194102 (2005)

Group PolyPhotonique

Hollow Photonic Crystal Fiber (PCF) versus Holey Fiber Absorption Based Sensors

- Much larger fraction (compared to HFs) of the core mode power is located within the hollow core ~90-99%
- Much larger compared to HFs (while still very small) gas volumes are used for measurement (millilitres), increasing sensitivity
- Gas filling time of hollow PCFs under pressure is much smaller (~1-5 min) than that of HFs (~200min) due to a much larger PCF core size
- Hollow core PCFs can be designed to operate at almost any wavelength as bulk material losses of their constituent materials are greatly suppressed due to modal propagation in the hollow core
- Effectively single mode operation allows reliable sensing only in a finite bandwidth window of operation, while HFs are considerably more broadband
- Modal propagation loss of a core mode in PCFs is typically higher than that of HFs (dB per meter range)
- Fabrication of PCFs is considerably more difficult than HFs

Sensing Using Gas Filled Hollow Core Photonic Band Gap Fibers

f=98 % of the guided mode field energy can propagate in the air regions of the gas filled fiber

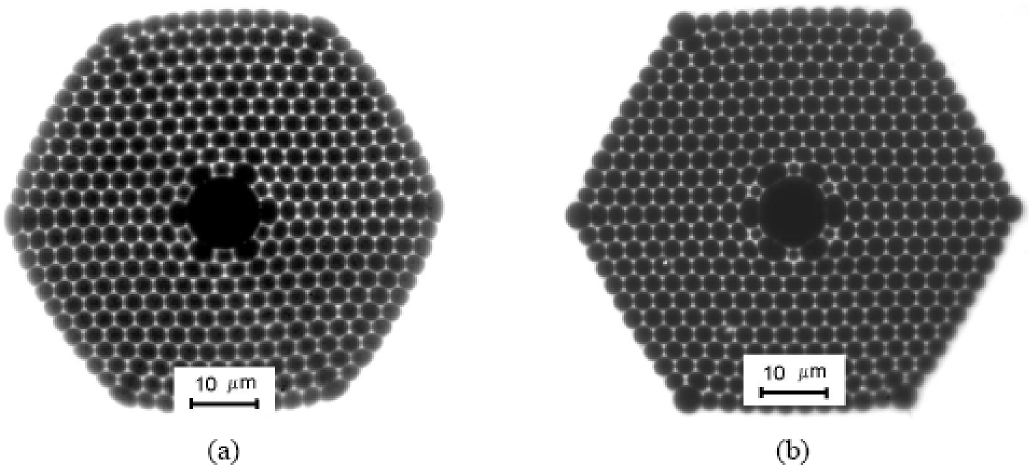

Fig. 1. Microscope images of (a) PBF1300 and (b) PBF1500.

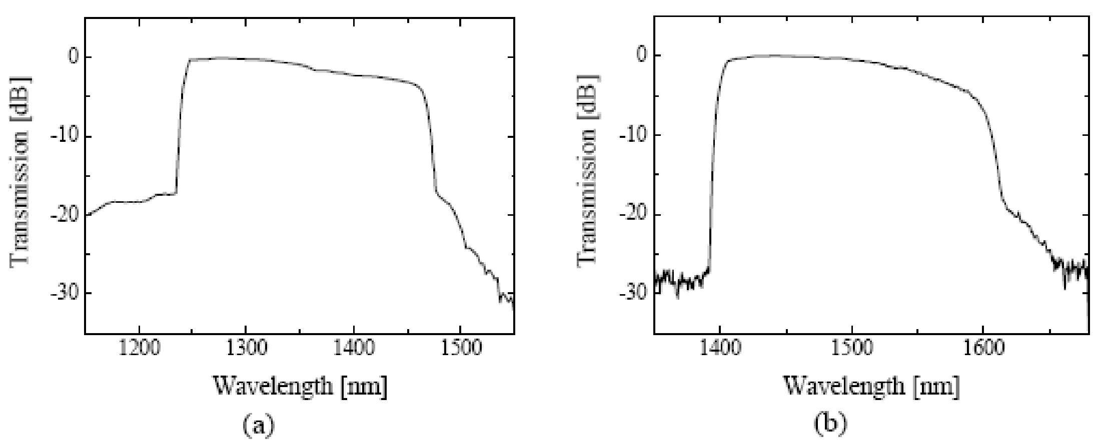

Fig. 2. Spectral transmission of (a) a 2 m long PBF1300 and (b) a 3 m long PBF1500.

Fiber propagation losses:

a) 0.1 dB/m
b) 0.2 dB/m

Effectively single mode regime in a limited bandwidth window ~2μm

T. Ritari et al., "Gas sensing using air-guiding photonic bandgap fibers," Opt. Express **17**, 4080 (2004)

LED+OSA vs. Tunable Laser Source

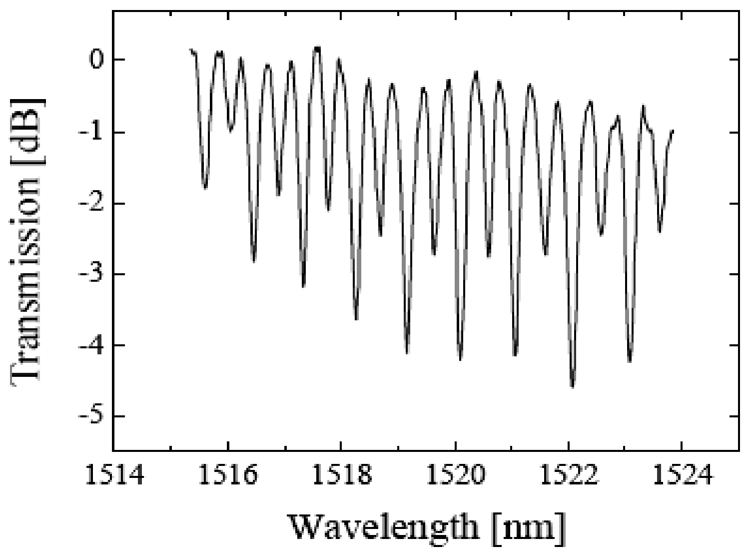

Fig. 8. Normalized absorption spectra of R-branch of $^{12}C_2H_2$ in a 1 m long PBF1500 measured using a LED. The resolution of the OSA is 0.1 nm. The lines appear broader due to the limited resolution of the OSA.

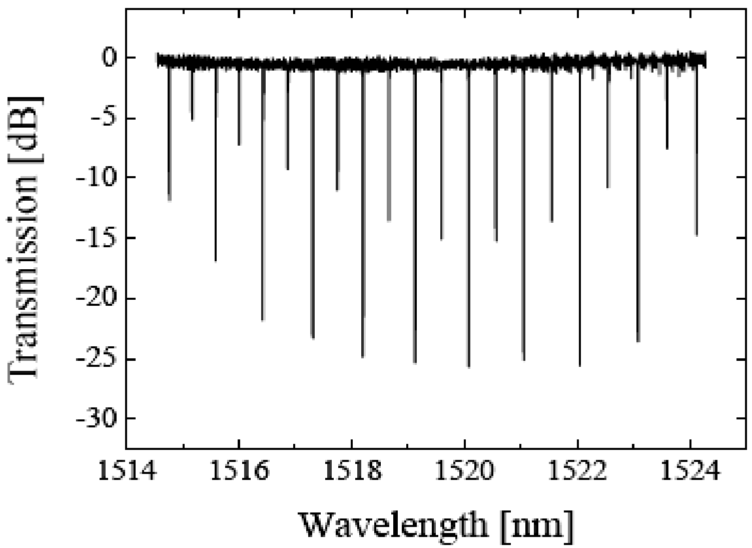

Fig. 9. For comparison, the same spectrum recorded using a laser (step size 1 pm) and a reduced pressure of 10 mbar.

T. Ritari et al., "Gas sensing using air-guiding photonic bandgap fibers," Opt. Express **17**, 4080 (2004)

Liquid Core Microstructured Fibers

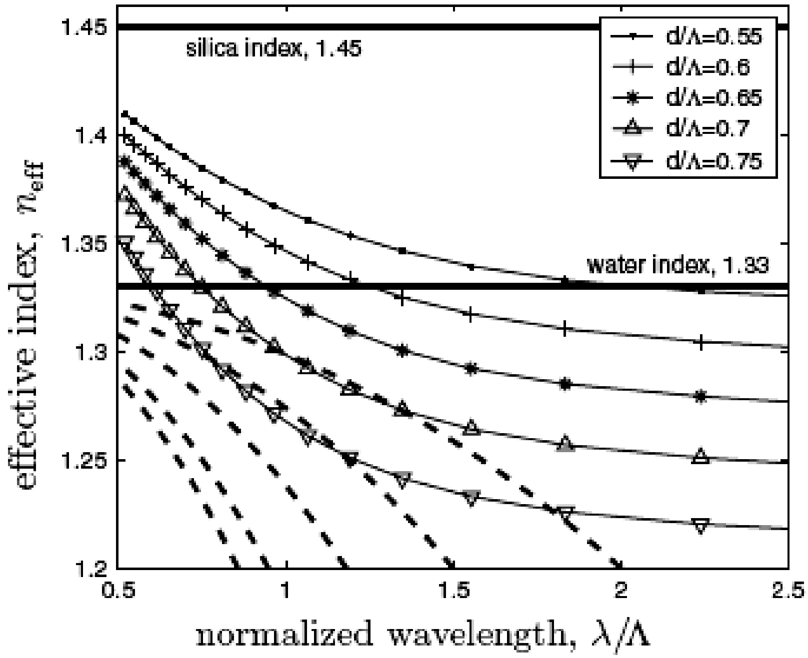

Figure 8. For high enough air-fill-fraction, the average index of a silica–air cladding can drop below the index of water, allowing index-guidance of light in a water core. The average index is here quantified by the wavelength-dependent total-internal-reflection edge, $n_{\mathrm{TIR}}(\lambda)$, which crosses $n_{\mathrm{water}} \approx 1.33$ for all d/Λ greater than around 0.54. Also shown are analytical mode line estimates (dashed), suggesting that strong confinement of light in the water core will require d/Λ values closer to 0.7.

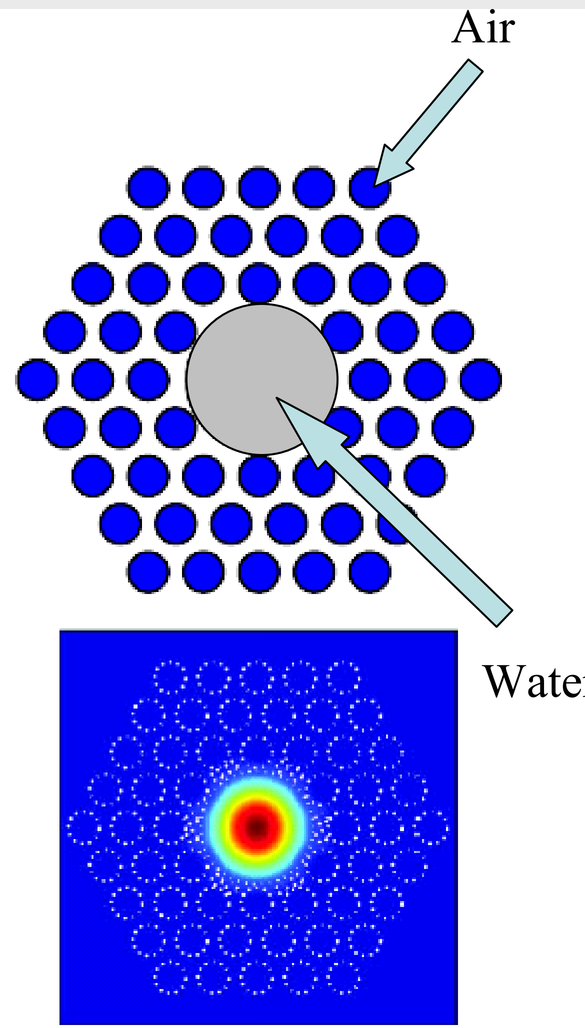

J.M. Fini, "Microstructure fibres for optical sensing in gases and liquids," Meas. Sci. Technol. **15**, 1120 (2004)

Liquid Core All-Polymer Bragg Fibers

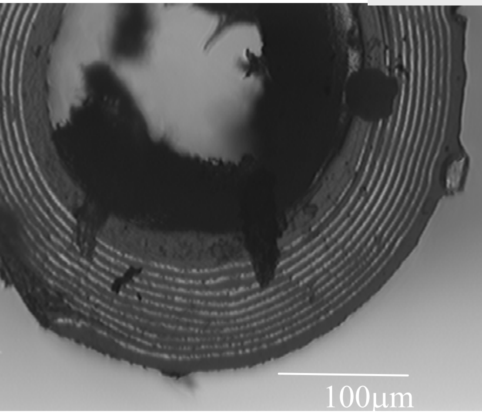

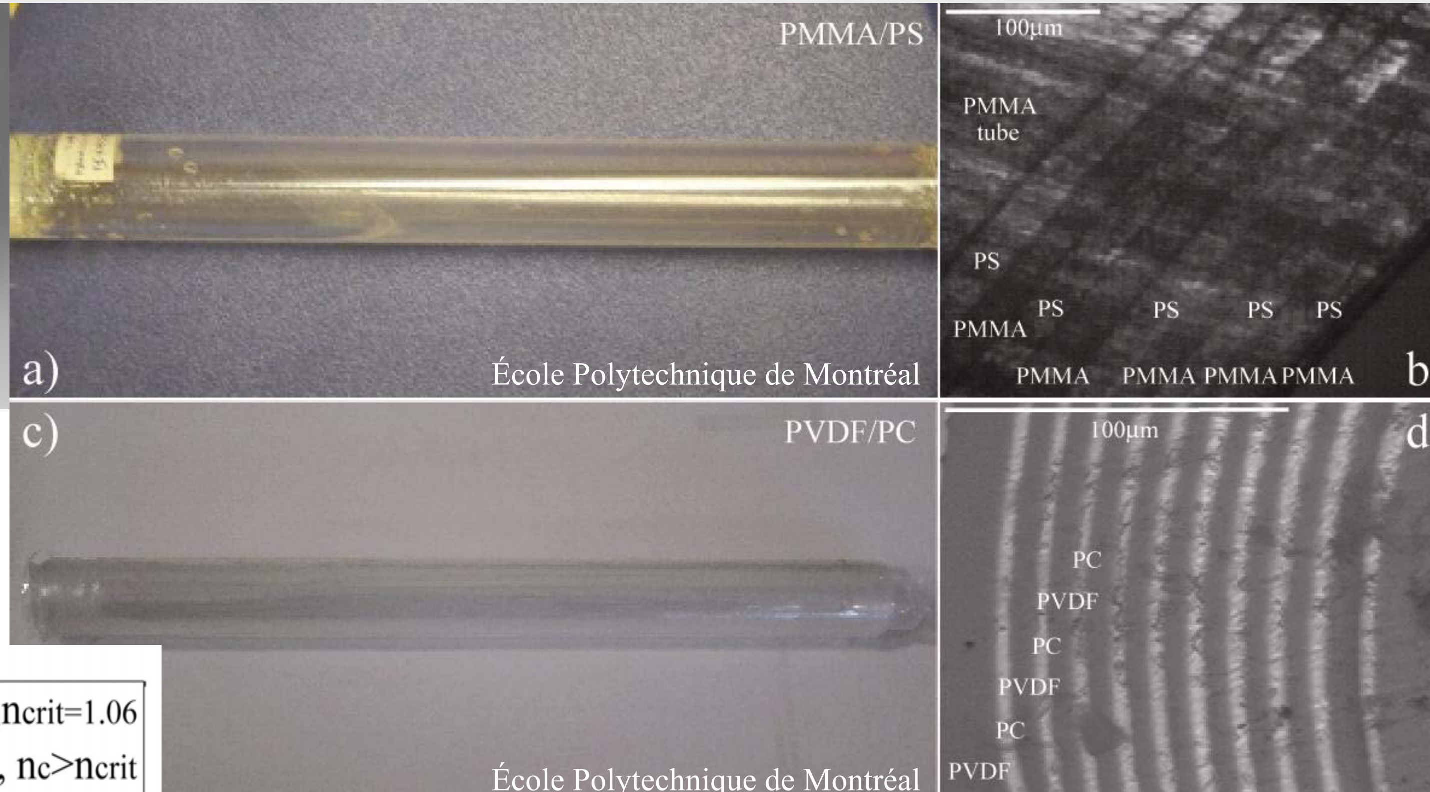

M. Skorobogatiy
École Polytechnique
de Montréal

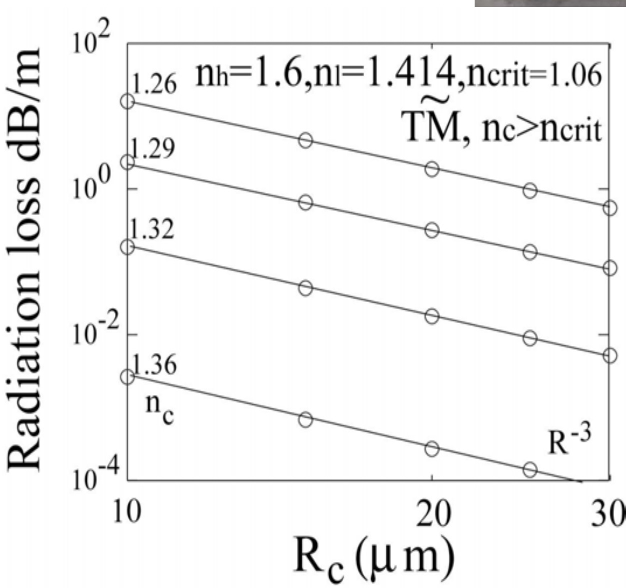

Theoretical loss of a water filled core guide
n_h/n_l=1.6/1.42, R_c=10μm, λ=1μm, is 0.2dB/m

M. Skorobogatiy, "Efficient anti-guiding of TE and TM polarizations in low index core waveguides without the need of omnidirectional reflector," Opt. Lett. **30**, 2991 (2005)

M. Skorobogatiy et al., "Consecutive Solvent Evaporation and Co-Rolling Techniques for Polymer Multilayer Hollow Fiber Preform Fabrication," accepted for publication in the Journal of Materials Research 2006.

Temperature and Stress Change Sensors

Temperature Sensing with Holey Fibers Using Direct Interferometric Methods

A resultant change of the refractive index of silica (Δn_{Si})and the phase change ($\Delta\phi$) connected with the temperature change can be written as:

$$\Delta n_{Si} = \gamma \cdot \Delta T \tag{3}$$

$$\Delta\phi = k \cdot n_{eff} \cdot L \cdot \alpha \cdot \Delta T + k \cdot L \cdot (n_{eff1} - n_{eff}) \tag{4}$$

where γ is the thermo-optic coefficient, α is the thermal expansion coefficient and n_{eff} and n_{eff1} are the effective refractive indices before and after temperature change, respectively.

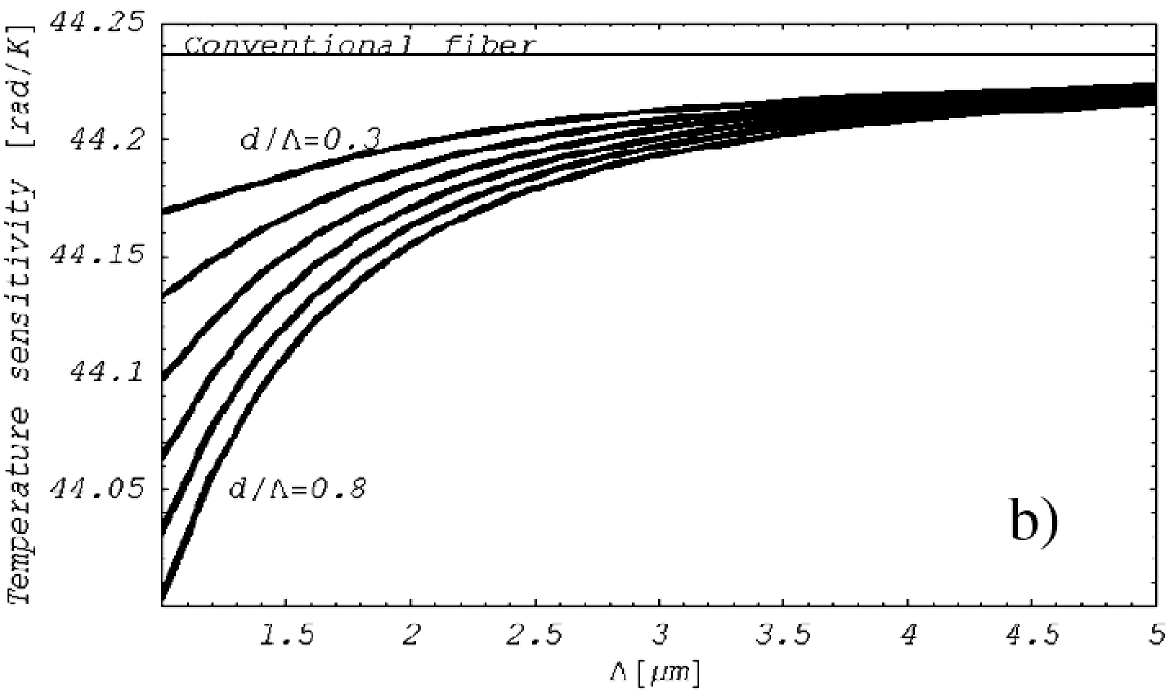

Temperature and elongation sensitivities of HFs are somewhat lower than sensitivities of the conventional step-index fiber

N. Palka, "Sensing properties of photonic crystal fibers," J. Phys. IV France **129**, 143 (2005)

ÉCOLE POLYTECHNIQUE MONTRÉAL

Polarimetric Optical Fiber Sensors

Polarimetric optical fiber sensors rely on the modulation of the state of polarization of the optical signal as a function of external perturbations (e.g., temperature, strain, stress or hydrostatic pressure, etc.). These sensors mainly involve polarization maintaining (birefringent) fibers.

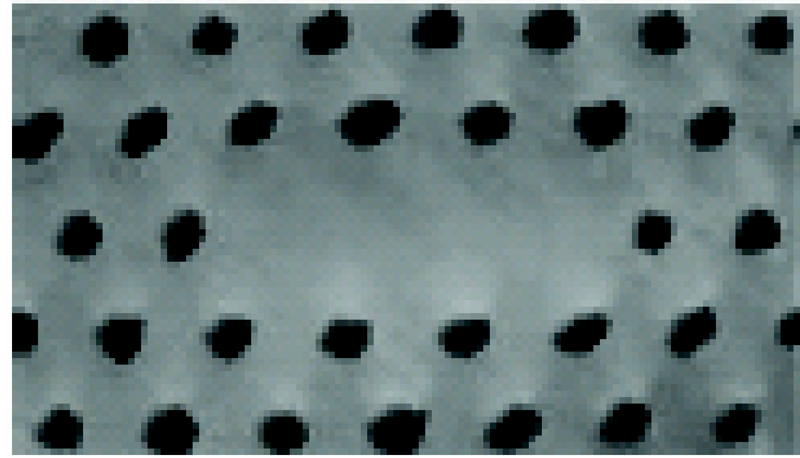

Geometrical birefringence of the order of $7 \cdot 10^{-3}$ may be induced in photonic crystal holey fibers, while in conventional highly birefringent fibers that reach only $5 \cdot 10^{-4}$ by employing stress-applying elements.

One of the crucial factors impacting the applicability of birefringent fibers to specific sensing applications is their polarimetric sensitivity to temperature. Such sensitivity of HFs is an order of magnitude lower than that in regular PMFs beacause of the absence of stress inducing regions in HF structure.

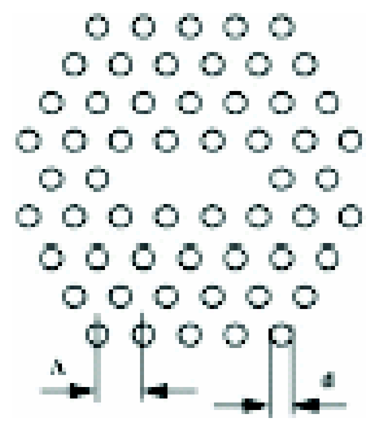

Moreover, HF based PMFs can be designed to further lower their temperature sensitivities making them several orders of magnitude lower than in traditional PMFs.

T. Martynkien et al., “Modeling and measurement of temperature sensitivity in birefringent photonic crystal holey fibers,” Appl. Opt. 44, 7780 (2005)

Group PolyPhotonique

Designing of Temperature-Desensitizes Highly Birefringent Holey Fibers

Thermal properties of birefringent fibers are characterized with a parameter known as polarimetric sensitivity to temperature, which is defined as:

$$K_T = \frac{d\Delta\varphi}{dTL} = \frac{2\pi}{\lambda}\left(\frac{dB}{dT} + B\alpha\right),$$

Where thermal expansion coefficient is α, thermo-optic coefficient is γ, And birefringence is defined as:

$$B = \frac{\lambda}{2\pi}(\beta_x - \beta_y)$$

Dominant term is silica glass which has to be minimized by geometrical design

$$K_T(\lambda) = \frac{2\pi}{\lambda}\left[\frac{dB(\lambda)}{dn_{\mathrm{glass}}}\gamma_{\mathrm{glass}} + \frac{dB(\lambda)}{dn_{\mathrm{hole}}}\gamma_{\mathrm{hole}} + \frac{dB(\lambda)}{d\Lambda/\Lambda}\alpha_{\mathrm{glass}} + B(\lambda)\alpha_{\mathrm{glass}}\right].$$

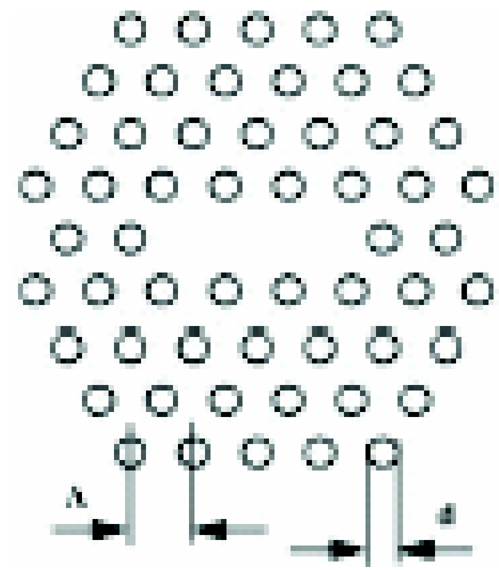

T. Martynkien et al., "Modeling and measurement of temperature sensitivity in birefringent photonic crystal holey fibers," Appl. Opt. 44, 7780 (2005)

ÉCOLE POLYTECHNIQUE MONTRÉAL

Reduced Temperature Sensitivity of Specialty Design Highly Birefringent HFs

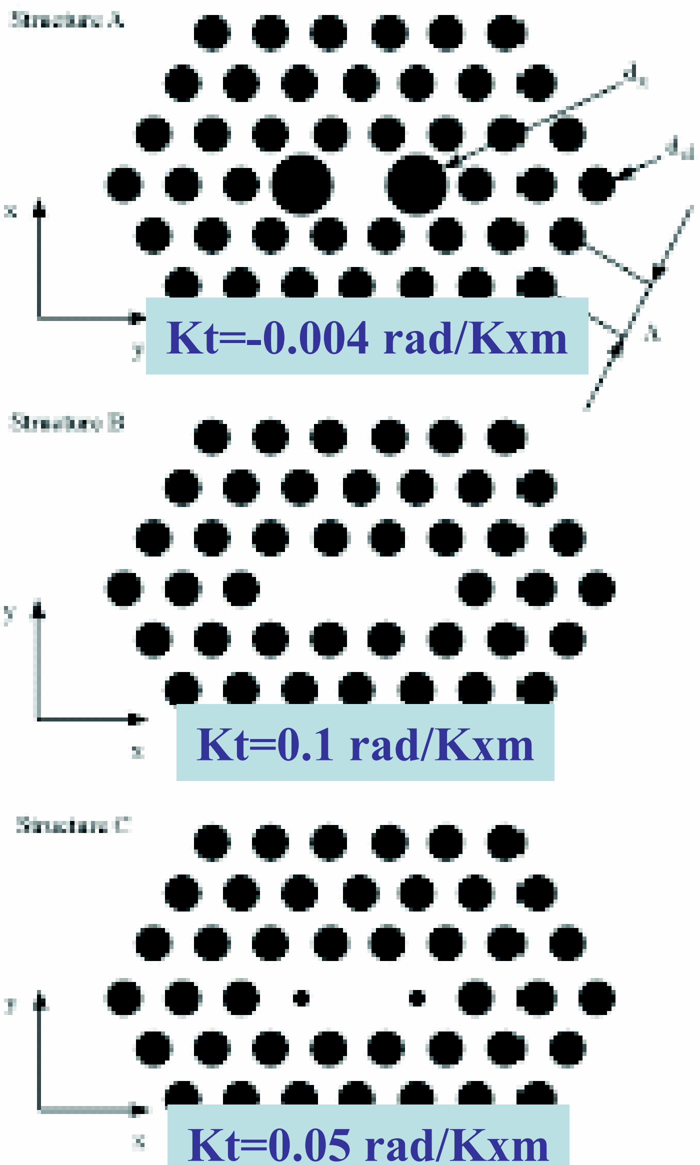

Fig. 1. Cross sections of the birefringent holey fibers.

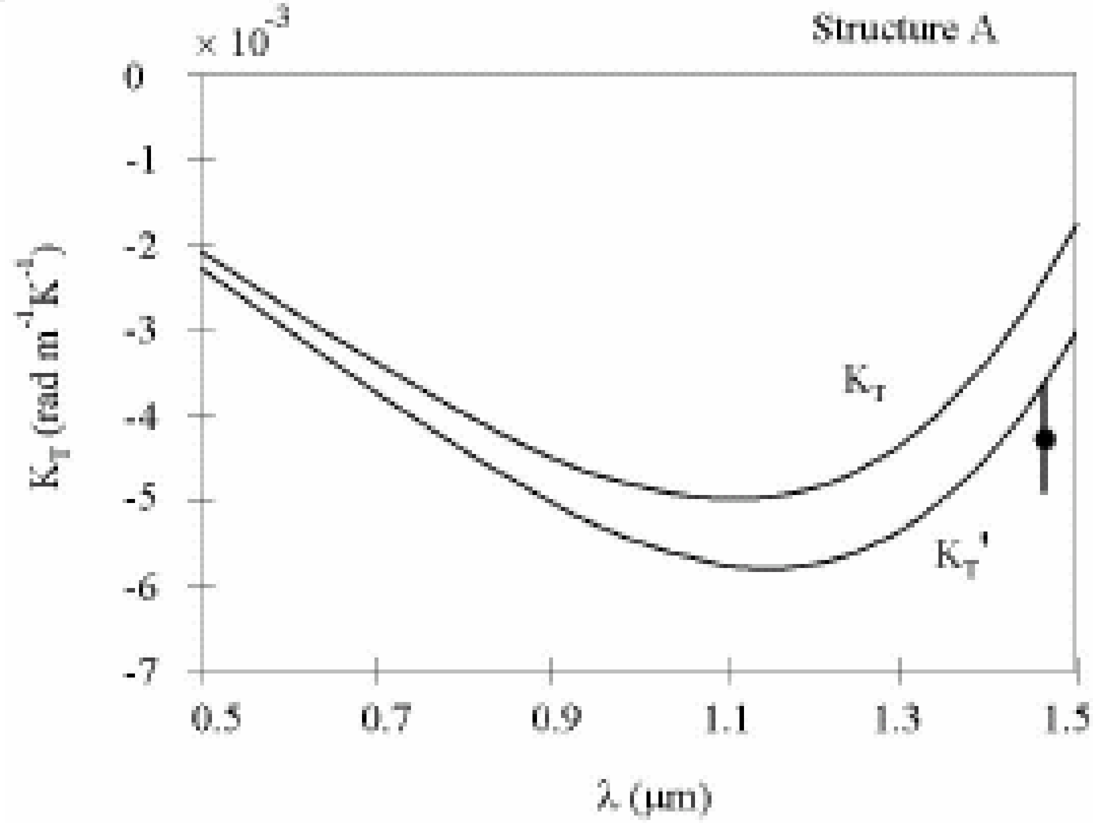

Compare with sesitivities of:
0.5 rad/Kxm in elliptical core fibers
5.0 rad/Kxm in fibers with stress-applying elements

PolyPhotonique Group

ÉCOLE POLYTECHNIQUE MONTRÉAL

Tunable Photonic Band Gap and Heat Sensing

Upon placing a high index liquid n =1.80 into the holes Figure 1, a strongly wavelength dependent Band Gap guidance is observed, Figure 2.

Holes infiltrated with liquid crystal n=1.8

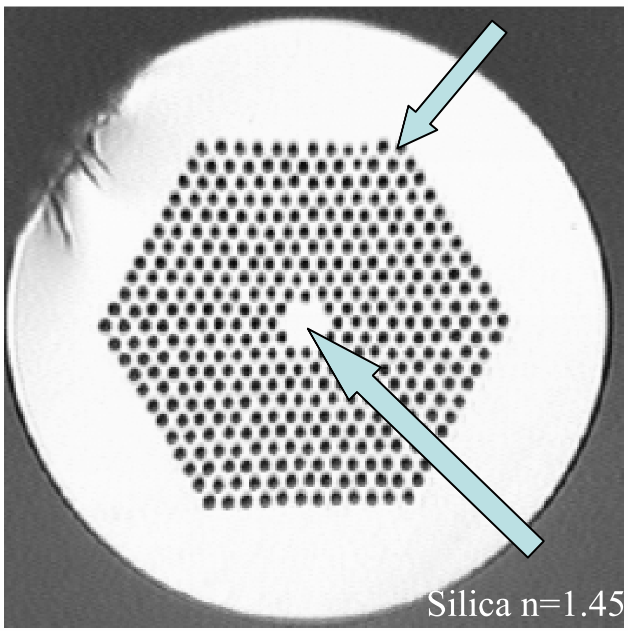

Cross-section of the sol-gel derived photonic band gap fiber.

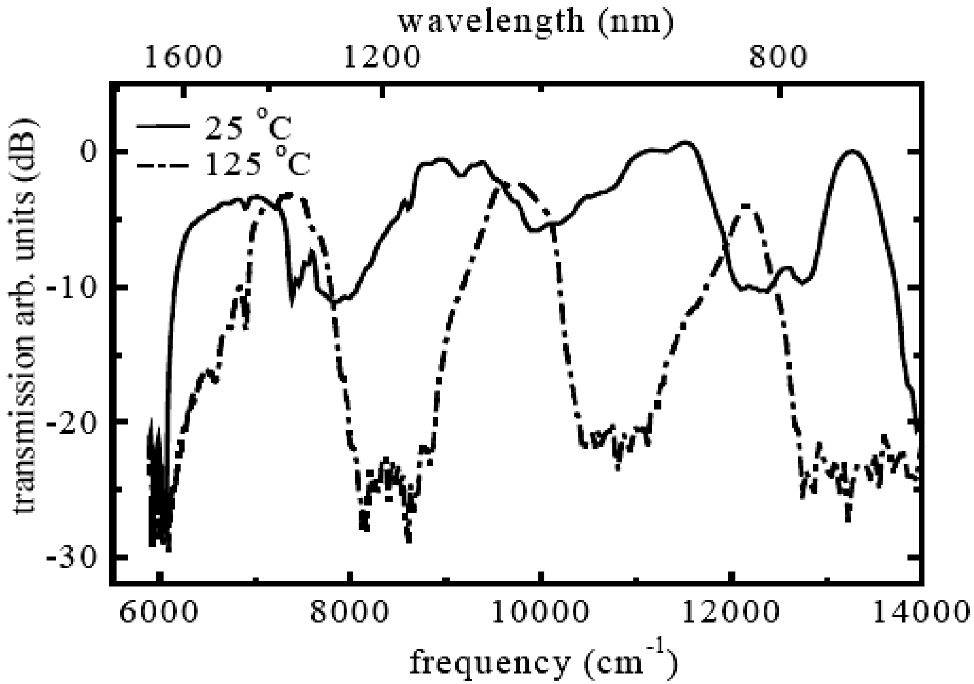

Fig 2. Tranmission spectra of the Photonic Band Gap fiber show in Fig 1. when the air-holes are filled with a liquid having an index of 1.80. The spectrum taken at 25°C and 125 °C are shown with solid and dot-dashed lines respectively.

R. Bise et al., "Tunable photonic band gap fiber," OFC ThK3 (2002)

Grou PolyPhotonique

Tunable Photonic Band Gap and Heat Sensing

A Photonic Crystal Fiber has been filled with a cholesteric liquid crystal. A temperature sensitive Photonic Band Gap effect was observed, which was especially pronounced around the liquid crystal phase transition temperature.

The bands have a temperature sensitivity of approximately 2.5-3nm/°C from 25°C to 75°C. Above 75°C the band structure begins to change and changes drastically when the temperature approaches TC

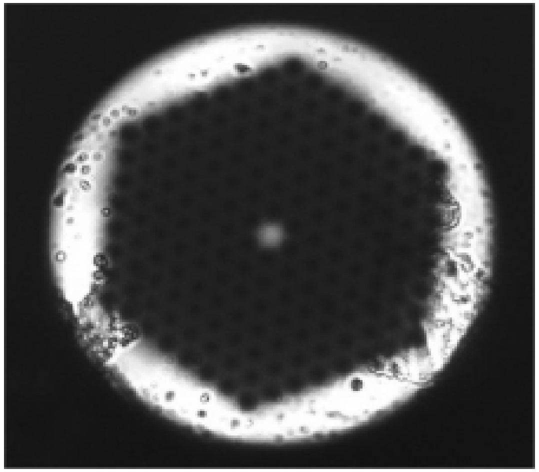

Figure 1 End facet of a Photonic Crystal Fiber where green light is guided by the Photonic BandGap effect.

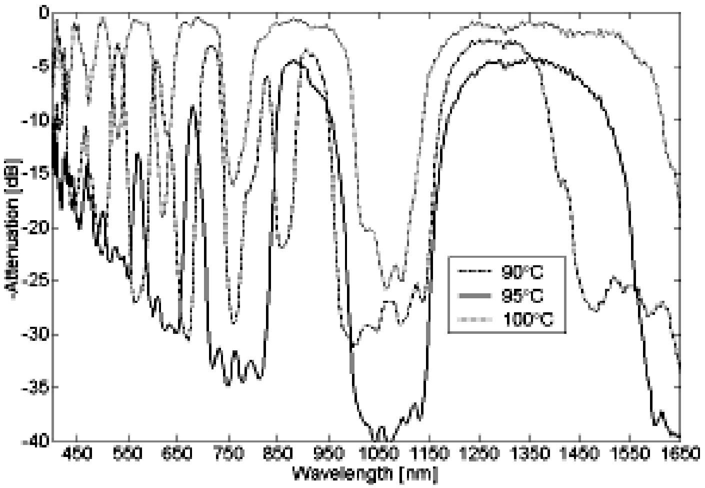

Figure 3 Normalized transmission spectra for the filled PCF at 90°C, 95°C and 100°C.

T.T. Larsen et al., "Tunable photonic band gaps in PCFs filled with cholesteric liquid crystal ," ECOC (2003)

Stimulated Brillouin Scattering to Measure Strain and Temperature

- Simple explanation of a Stimulated Brillouin Scattering
  - Pump generate an "acoustics Phonon"
  - Acoustic wave modulates the medium refractive index
  - pump induced index grating scatters the pump through Bragg diffraction

- SBS shift and amplitude are very sensitive to temperature and strain as these are the control parameters of the phonon properties
- The spectral width of gain spectrum related to damping time of acoustics wave or the "acoustics phonon" life time

$$\nu_B = \Omega_B / 2\pi = 2n v_A / \lambda_p$$

$$\lambda_p = 1.55\,\mu m, \quad n = 1.45, \quad v_A = 5.96\ km/s \ \Rightarrow \ \nu_B \approx 11\,GHz$$

$$acoustic\ wave\ \ decay \propto \exp[-\Gamma_B t]$$

$$phonon\ lifetime: \ T_B = \Gamma_B^{-1} \approx 10\,ns$$

G.P. Agrawal , Nonlinear fiber optics, Academic press, 1995

Enomori I, Saitoh K, Koshiba M, ''Fundamental characteristics of localized acoustic modes in photonic crystal fibers,'' IEICE Trans. Electr. E88C, 876 (2005)

Group PolyPhotonique

SBS Holey Fiber Sensors

The simultaneous measurement of temperature and strain is not directly possible for the usual Brillouin based sensors with a single-mode fiber because the Brillouin spectrum has only one peak whose frequency is sensitive to both temperature and strain variations.

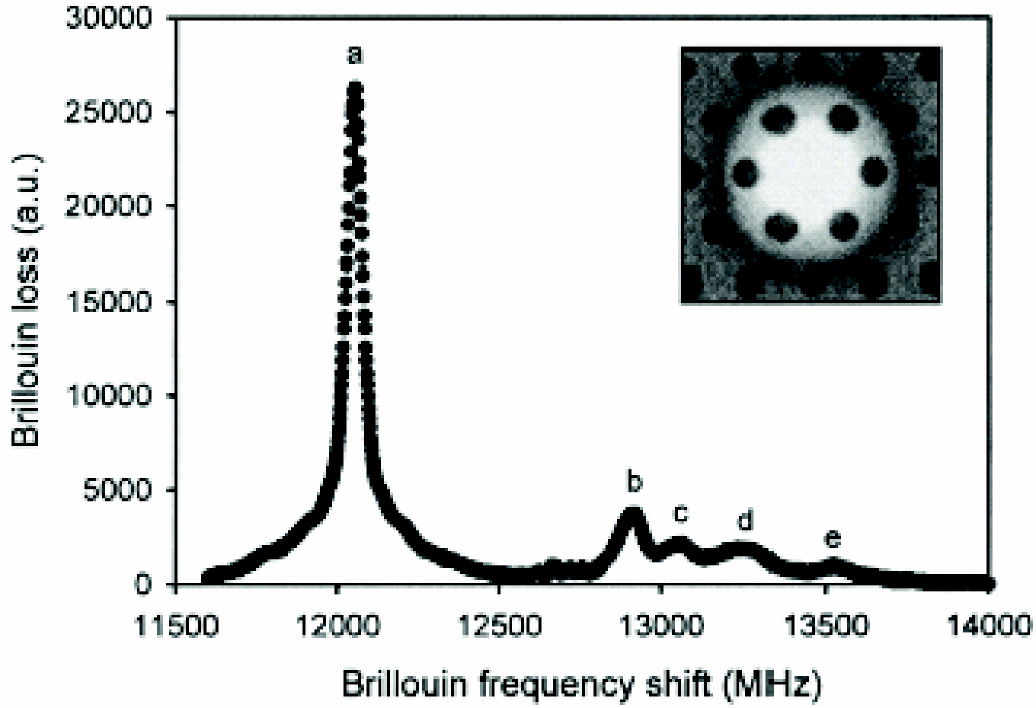

Solution: multicomposition fiber core that results in a multipeak Brillouin spectrum.

For a HF the temperature and strain coefficients are different for two Brillouin peaks that originated from two different materials of the core.

The PCF has a 2.3 mm-diameter solid silica core that comprises a 0.8-mm-diameter Ge-doped center region with a parabolic refractive index profile.

Peaks a and c are due to the scattering from longitudinal acoustic waves in the Ge-doped center region and the solid pure-silica region of the core, respectively.

L. Zou et al., “Dependence of the Brillouin frequency shift on strain and temperature in a photonic crystal fiber,” Opt. Lett. **29**, 1485 (2004)

SBS Holey Fiber Sensors

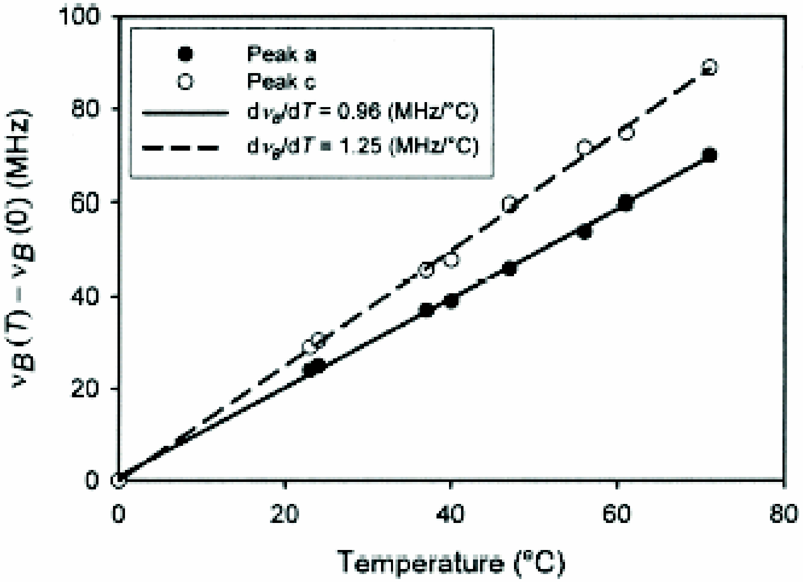

Fig. 2. Central frequencies of peaks a and c as functions of temperature. $[\upsilon_B(T) - \upsilon_B(0)]$ is given by either $[\upsilon_B{}^{\mathrm{pk\,a}}(T) - \upsilon_B{}^{\mathrm{pk\,a}}(0)]$ or $[\upsilon_B{}^{\mathrm{pk\,c}}(T) - \upsilon_B{}^{\mathrm{pk\,c}}(0)]$.

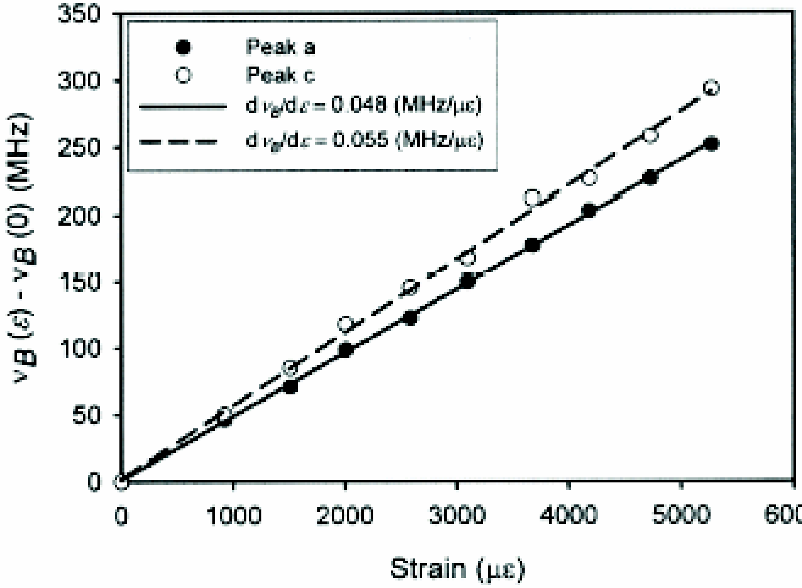

Fig. 4. Central frequencies of peaks a and c as functions of strain. $[\upsilon_B(\epsilon) - \upsilon_B(0)]$ is given by either $[\upsilon_B{}^{\mathrm{pk\,a}}(\epsilon) - \upsilon_B{}^{\mathrm{pk\,a}}(0)]$ or $[\upsilon_B{}^{\mathrm{pk\,c}}(\epsilon) - \upsilon_B{}^{\mathrm{pk\,c}}(0)]$.

Errors of temperature and strain are found to be:
Multicomposition HF: 3.9C and 83 με
These results show higher measurement accuracy compared with:
Multicomponent MMF: 27C and 570 με
SMF (T and strain contributions are hard to distinguish) 4.1C and 140 με
This difference may be attributed to the higher power density for a small core of the PCF, which results in higher Brillouin gain–loss and a better signal-noise ratio.

L. Zou et al., "Dependence of the Brillouin frequency shift on strain and temperature in a photonic crystal fiber," Opt. Lett. **29**, 1485 (2004)

Group PolyPhotonique

Resonant Sensors

Resonant multicore HFs for Sensing

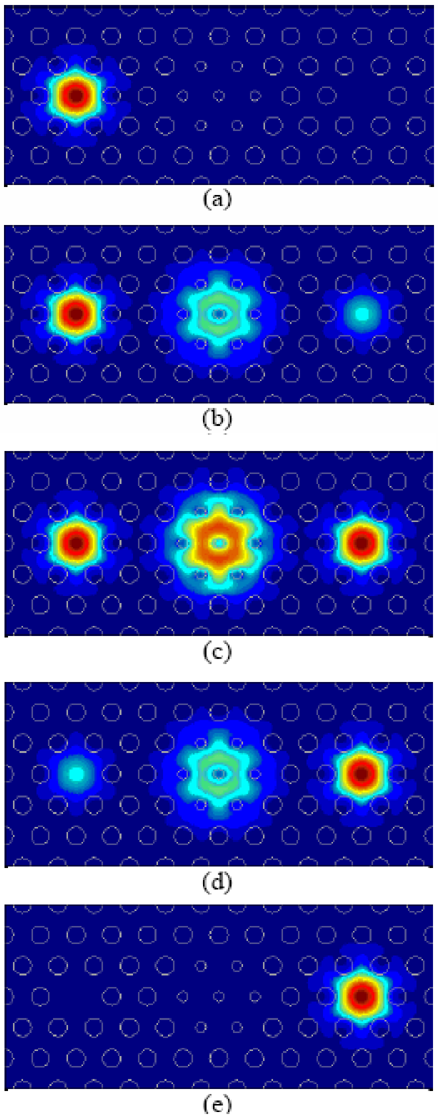

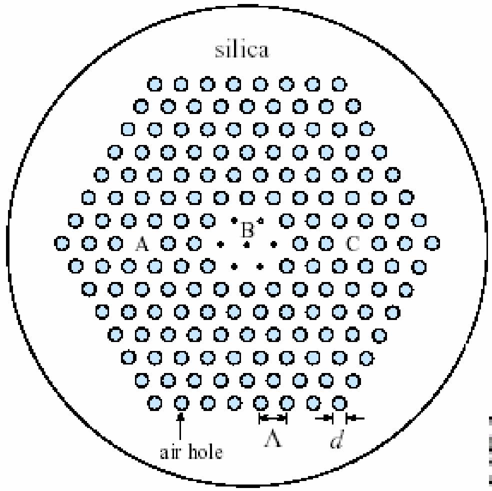

Shift in the resonance wavelength due to change in the analyte

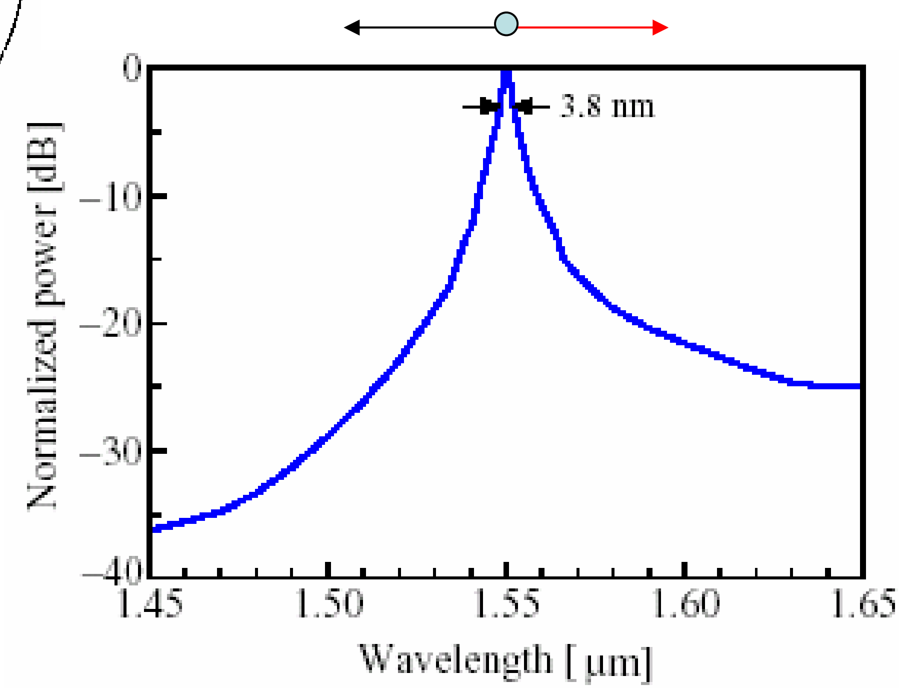

Fig. 5. Bandpass filtering characteristics of three-core PCF filter.

K. Saitoh, N.J. Florous, M. Koshiba, and M. Skorobogatiy, "Design of narrow band-pass filters based on the resonant-tunneling phenomenon in multicore photonic crystal fibers," Opt. Express **25**, 10327 (2005)

Group PolyPhotonique

Conclusions

- In PCFs it is the **geometry** rather than **properties** of the constituent materials that offers a versatile design parameter
- The holes in the cladding or a core of PCFs open up new opportunities for exploiting the interaction of light with gases and liquids via evanescent or direct coupling
- PCF geometry can be designed to enhance light-matter interaction – putting the light where the analyte is
- PCF geometry can be designed to reduce unwanted effects such as temperature sensitivity of fiber response
- PCF geometry can be designed to facilitate phase matching between the power guiding optical modes and resonant "sensing" modes such as plasmons

Acknowledgements

Prof. Masanori Koshiba (HU)

Dr. Kunimasa Saitoh (HU)

Prof. Charles Dubois (EPM)

Prof. Suzanne Lacroix (EPM)

Prof. Nicolas Godbout (EPM)

Dr. Andrey Kabashin (EPM)

PhD Alireza Hassani (EPM)

PhD Nicolaos Florous (HU)

MSc Ning Guo (EPM)

RA Yan Gao (EPM)

Post-Doc Elio Pone (EPM)

PhD Alexandre Dupuis (EPM)

(EPM) École Polytechnique de Montréal
(HU) Hokkaido University